Supplementary Information

on

Delayed coalescence dynamics in shear-thickening non-Brownian colloidal droplets

M. V. R. Sudheer,[1#] Sarath Chandra Varma,[2#] Aloke Kumar,[2] Udita U. Ghosh[1*]

[1]*Department of Chemical Engineering and Technology, Indian Institute of Technology (BHU), Varanasi, 221005, India.*

[2]*Department of Mechanical Engineering, Indian Institute of Science, Bangalore, 5610012, India.*

Contents:

1. Note S1 : Particle size distribution and surface tension of colloidal suspensions

Diluted suspensions (0.01 w/w %) were prepared to measure the particle size distribution of corn-starch particles. Droplets from these aqueous suspensions were allowed to dry on cleaned glass slides and then imaged using optical microscopy (*RADICAL, RXLr-5*) in transmission mode. **Fig. S1 (inset)** shows a representative optical microscopic image where individual corn-starch particles are visible. Several (~ 20) such microscopic images were acquired and analysed to evaluate the individual particle diameter and particle size distribution (**Fig. S1**) using Image J (v: 1.53k) software. The average particle diameter was found to be, $d_p\ (\mu m)$ ~ 15.29 ± 4.37.

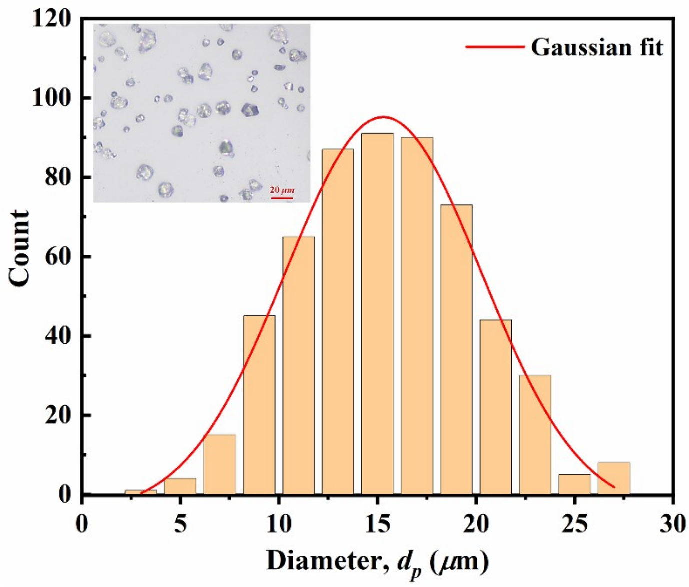

Fig. S1 Particle size distribution of corn-starch particles. Inset shows representative optical microscopic image of corn-starch particles under transmission mode.

The surface tension, $\sigma\ (mN/m)$ of the colloidal (corn-starch) suspensions were measured by pendant drop method using a goniometer (*Biolin Scientific,* Sweden, Theta lite). The surface tension for the suspensions $(\phi_w = 0\ to\ 0.41)$ investigated in this study were found to lie in the range 54 – 62 mN/m.

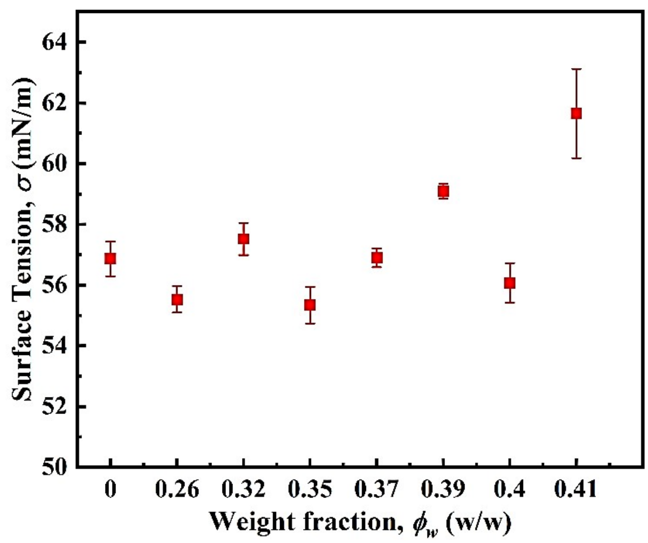

Fig. S2 Measured surface tension, $\sigma\ (mN/m)$ of the colloidal suspensions as a function of particle weight fraction, ϕ_w

2. Note S2 : Rheological characterization of colloidal suspensions

Table S1: Extracted parameters from Cross model fit $\mu(\dot{\gamma}) = \mu_\infty + \frac{\mu_o - \mu_\infty}{1 + (\Gamma\dot{\gamma})^n}$

Particle weight fraction, ϕ_w (w/w %)	Zero-shear viscosity, μ_o (mPa-s)	Infinite-shear viscosity, μ_∞ (mPa-s)	Time constant, Γ (s^{-1})	Power-law index, n	Viscosity at critical shear rate, μ_c (mPa-s)
0.32	15.1137	78.4276	0.00095	147	15.13
0.35	19.6519	175.2658	0.00093	1.65	18.83
0.37	18.1923	105.3562	0.00081	1.28	17.86
0.39	29.8911	300	0.00221	1.86	28.42
0.40	50.9698	500	0.00407	2.06	51.27
0.41	75.9886	580.7510	0.00583	2.76	74.90

Effect of measuring geometry

Variation of viscosity with shear rate obtained with two different geometries (cone-plate, filled symbols and parallel plate, open symbols) are shown in **Fig. S3** for three representative particle weight fraction – 0.26, 0.35, 0.4. Triplicates pertaining to each geometry are represented as Trial 1, Trial 2 and Trial 3. It must be noted that range of shear rate with the cone and plate geometry (plate diameter : 40 mm, cone angle $1°$) is $\dot{\gamma}$ ($10^{-2} - 10^{3}\ s^{-1}$) while for the parallel plate geometry (plate diameter : 25 mm) the imposed shear rate, $\dot{\gamma}$ ($10^{0} - 10^{3}\ s^{-1}$).

(i) $\phi_w \sim 0.26$: The profiles superimpose in the common range of shear rate, $\dot{\gamma} \sim 10^{0} - 10^{2}\ s^{-1}$

(ii) $\phi_w \sim 0.35$: Both the geometries exhibit similar trend that comprises of a shear thinning behavior at low shear rate followed by shear thickening beyond the critical shear rate.

(iii) $\phi_w \sim 0.4$: The effect of particle content significantly reflects on the viscosity measurements where the profiles differ significantly in terms of zero shear viscosity values for between the two geometries. This deviation could arise for myriad reasons such as confinement effect, particle migration and slip at the wall of plate as well as detection limit or sensitivity of the rheometer.[1] The profiles however, superimpose for $\dot{\gamma} > 10^{0}$ implying the viscosity measurements are consistent across both geometries. Similar system was characterised by Fall et al.,[2] albeit in

Couette geometry and the critical shear rate for transition to shear thickening was $\dot{\gamma}_c \sim 10\ s^{-1}$ for $\phi_w \sim 0.35$ that differs by an order, $\dot{\gamma}_c \sim 2-3\ s^{-1}$ in the present report. This implies that while deviations may arise in exact values of measured viscosity and critical shear rate but the existence of shear-thinning and shear-thickening regimes is consistent.

(iv) It must also be noted that the data utilised in the proposed theoretical model is based on the cone-plate geometry and pertaining to the range of shear rate consistent with coalescence process, $O(10^1)\ to\ O(10^3)$

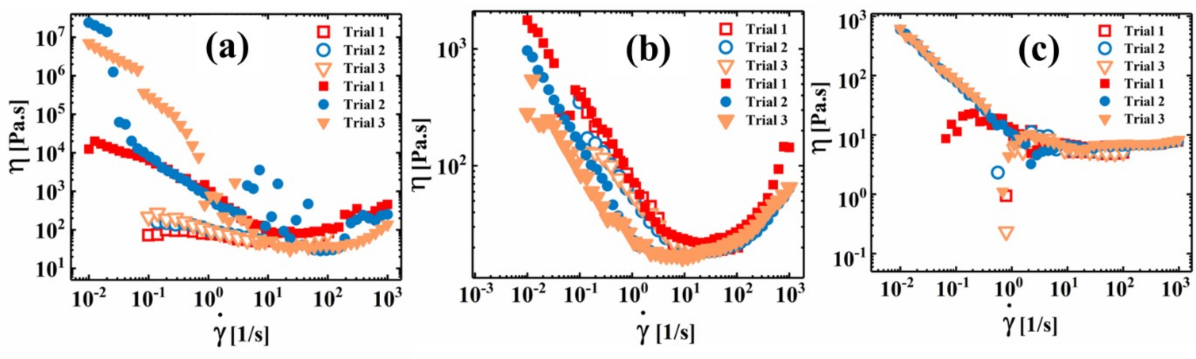

Fig. S3 Variation of suspension viscosity with shear rate to outline the effect of geometry employed for measurement. Here, open and filled symbols indicate measurements taken with parallel plate and cone-plate geometry respectively for particle weight fraction, ϕ_w corresponding to **(a)** 0.4 **(b)** 0.35 **(c)** 0.26.

3. Note S3 : Determination of region of interest

Coalescence phenomenon comprises of four morphological stages as initial contact (I), film drainage (II), film rupture (III) and merging (IV). At the onset of coalescence, i.e., the initial contact (I) between the sessile and pendant droplet interfaces is a single point. This singular point is beyond detection as per the spatial resolution of the camera. Beyond this point, the interface can be represented by a flat line (**Fig. S4,** $t \sim 10^{-4}$). This is followed by the formation of the liquid bridge (II, III) between the two droplets (sessile and pendant) that manifests in the form of curvature change or neck formation. The exponential increase in neck radius, R that is the growth of the neck radius forms the region of interest (ROI) in the present study. On a logarithmic scale, it can be defined by the relation, $R \sim t^b$ corresponding to the linear portion as shown in **Fig. S4 (inset)**. Therefore, although the coalescence phenomenon is of few orders of magnitude, $10^{-5} - 10^{-2}\ s$ but the region of interest (merging, IV) that can be studied is limited to a single order of magnitude

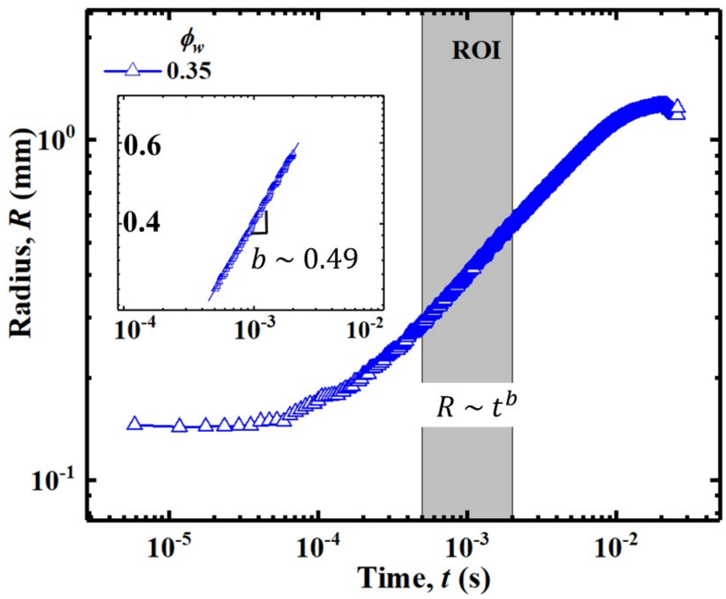

Fig. S4 Evolution of the neck radius, R (mm) corresponding to colloidal suspension with particle weight fraction, $\phi_w \sim 0.35$ with the region of interest that is the focus of the present study. Inset shows the blow of the region-of-interest (ROI) where, $R \sim t^b$ is applicable with b as the power law exponent.

Detection of limits of the region of interest (ROI) via image processing depends on the resolution of the imaging device. The point of initiation in the present study is marked by the first image where 'quantifiable' neck radius is observed in the images. For example, for coalescing droplets of deionised water (DW), a marked increase in neck radius could be detected at Image-1143 (**Fig. S5**).

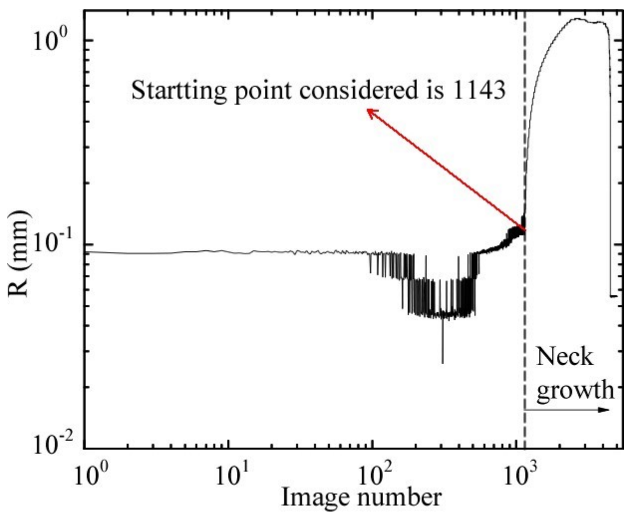

Fig. S5 Determination of coalescence initiation point via image processing. Here, R (mm) is the neck radius of coalescing water droplets corresponding to the image number.

By adopting Image-1143 as the reference for the initial point, the evolution of neck radius is depicted using black squares in **Fig. S6 (a)**. Next, we check if this method of initiation point detection has a bearing on the magnitude of the power law exponent in neck radius evolution. Therefore, the neck radius evolution is evaluated with different initiation points, Image-1133 and Image-1123), denoted by circle (red) and blue triangle (blue) respectively in **Fig. S6 (a)**. This shift in the choice of reference point for analysis introduced a marginal deviation, b = 0.504; 0.523 resp.

compared to b = 0.488 for Image-1143. It is worth noting that these deviations in 'b' lie well within the reported error margin of 10%.

The exercise was repeated for colloidal suspension droplets, $\phi_w = 0.4$. In this context, Image-207 serves as the initiation point and corresponding neck radius evolution is shown (**Fig. S6 (b)**) using squares (black). This resulted in the power law exponent, b = 0.281 for $\phi_w = 0.4$. Thereafter, shifting the initiation point to Image-197 and Image-187 altered b to 0.288 (circle, red) and 0.298 (triangle, blue) resp. in **Fig. S6 (b)**. Thus, the altered value of the power law exponent in neck radius evolution due to the choice of initial point remained within the bounds 10% error.

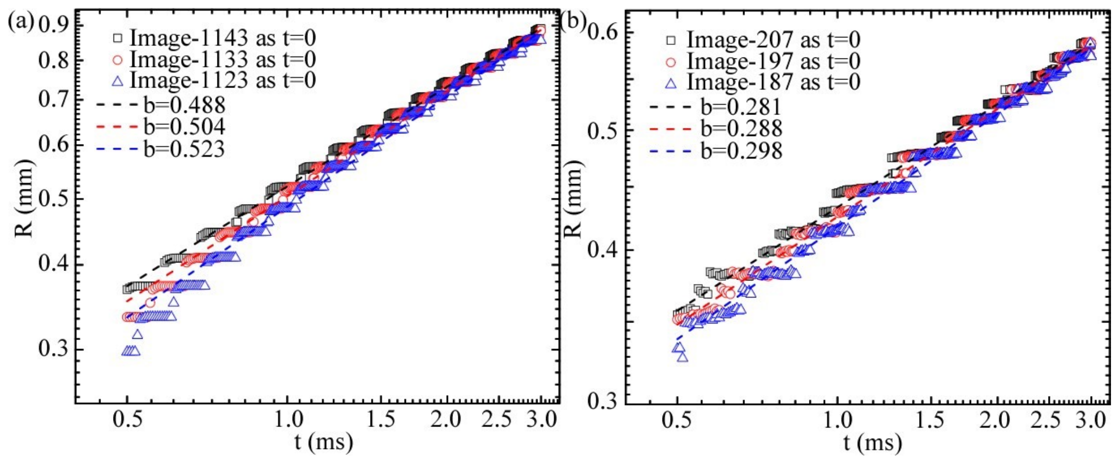

Fig. S6 Neck radius evolution in region of interest for varying coalescence initiation point for fluids **(a)** de-ionised water and **(b)** colloidal droplet $\phi_w = 0.4$.

4. Note S4 Estimation of fluid velocity through porous particle assemblies

Table S2: Parameter values employed for estimation of fluid velocity through porous particle assemblies

Parameter	Value	Order of magnitude
Surface tension of the suspension, σ	$0.059\ N/m$	10^{-2}
Filament diameter, D	$100\ \mu m$	10^{-4}
Modified Carman-Kozeny coefficient, k	$4\times\ 10^{-3}$	10^{-3}
Particle radius, a	$7.5\times\ 10^{-6}\ m$	10^{-14}
Viscosity, μ	$1\ Pa.s$	10^{0}
Velocity, u	$1.32\times\ 10^{-6}\ m/s$	10^{-6}

5. Note S5 : Scaling constants employed in theoretical model

Table S3: Parameter values of scaling constants employed in theoretical model

ϕ_w	C_1	C_2
0.26	-0.3	0.3
0.32	-0.3	0.3
0.35	-0.3	0.3
0.37	-0.3	5
0.39	-3	10
0.4	-5	15
0.41	-8	40

6. Note S6 : Peclet number variation with particle weight fraction

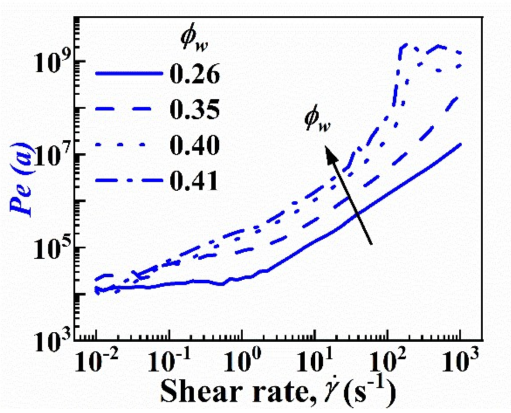

Fig. S7 Variation of Peclet number, $Pe\ (a)$ with imposed shear rate, $(\dot{\gamma})$ for representative particle weight fractions, $\phi_w \sim$ 0.26, 0.35, 0.4 and 0.41.

References :

1. Ewoldt, R.H., Johnston, M.T., Caretta, L.M. (2015). Experimental Challenges of Shear Rheology: How to Avoid Bad Data. In: Spagnolie, S. (eds) Complex Fluids in Biological Systems. Biological and Medical Physics, Biomedical Engineering. Springer, New York, NY.
2. A. Fall, F. Bertrand, D. Hautemayou, C. Mezière, P. Moucheront, A. Lemaître and G. Ovarlez, *Phys. Rev. Lett.*, 2015, **114**, 098301.